Analytica Chimica Acta 1207 (2022) 339817

Contents lists available at ScienceDirect

Analytica Chimica Acta

journal homepage: www.elsevier.com/locate/aca

Advancement of dengue virus NS1 protein detection by 3D-nanoassembly complex gold nanoparticles utilizing competitive sandwich aptamer on disposable electrode

Indra Memdi Khoris [a], Fahmida Nasrin [b], Ankan Dutta Chowdhury [b, 1], Enoch Y. Park [a, b, *]

[a] Department of Bioscience, Graduate School of Science and Technology, Shizuoka University, 836 Ohya Suruga-ku, Shizuoka, 422-8529, Japan
[b] Research Institute of Green Science and Technology, Shizuoka University, 836 Ohya Suruga-ku, Shizuoka, 422-8529, Japan

HIGHLIGHTS

- Aptamer biosensor based on the duplex formation as linker of 3D-nanoassembled AuNPs on disposable screen-printed electrode.
- Promoting 3D-nanoassembled AuNPs enabling a clear plasmonic shift and molecular carrier function.
- Dual-detectable visually naked-eye readout and sensitive electrochemical readout for low concentration of analyte.
- Detectable Dengue virus NS1 down to 30 fg/mL equivalent to 1000 times higher sensitivity compared to available biosensor.

GRAPHICAL ABSTRACT

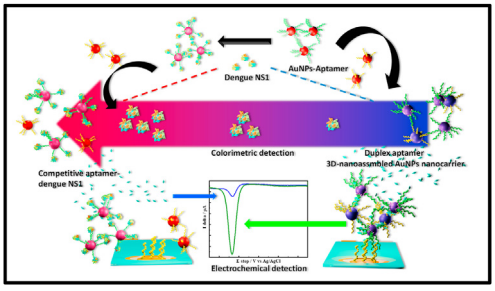

ARTICLE INFO

Article history:
Received 2 February 2022
Received in revised form
18 March 2022
Accepted 6 April 2022
Available online 9 April 2022

Keywords:
Gold nanoassembly
Aptamer biosensor
Colorimetric electrochemical
Dengue virus NS1
Redox nanocarrier

ABSTRACT

Signal amplification have been centralized in developing the highly reliable biosensor for analyte detection with a narrow detection window. We proposed an aptasensor to provide a highly sensitive early-stage diagnostic platform of dengue virus NS1 protein (DENV-NS1) by dual-approach – colorimetric and electrochemical detection. This work utilized two different aptamers specific to DENV-NS1: One conjugated to gold nanoparticles (AuNPs), forming AuNPs-Apt_1 and its complementary sequence aptamer, forming AuNPs-Apt_2. The unbound Apt_1 of AuNPs-Apt_1 by DENV-NS1 were to hybridize to AuNPs-Apt_2 and induced a 3D-nanoassembled formation, resulting in DENV-NS1 concentration-dependent plasmonic color change. Occurrence of the hybridization of Apt_1 and Apt_2, the 3D-assembled hybridized aptamers of AuNPs was incubated with methylene blue (MB) solution, which intercalated a high number of MB molecules within the duplex structure of aptamers, and the complex was captured on the Apt_2-conjugated disposable gold electrode (DGE). The developed aptamer-based biosensor showed high sensitivity with colorimetric response down to 1.28 pg/mL and electrochemical approach down to 30 fg/mL of DENV-NS1 with good selectivity. This work showcases an advanced utilization of aptamer and its complementary anti-sense aptamer in signal amplification and nanocarrier for biosensing.

* Corresponding author. Research Institute of Green Science and Technology, Shizuoka University, 836 Ohya, Suruga-ku, Shizuoka, 422-8529, Japan.
E-mail addresses: Indra.memdi.khoris.17@shizuoka.ac.jp (I.M. Khoris), Fahmida.Nasrin.17@shizuoka.ac.jp (F. Nasrin), dc_ankan@yahoo.co.in (A.D. Chowdhury), park.enoch@shizuoka.ac.jp (E.Y. Park).
[1] Current address: Amity Institute of Nanotechnology, Amity University Kolkata, Major Arterial Road (South-East), AA II, West Bengal 700135, India.

https://doi.org/10.1016/j.aca.2022.339817
0003-2670/

1. Introduction

In the last decades, dengue virus (DENV) infection has been a significant global health issue in tropical and sub-tropical countries worldwide [1]. This mosquito-borne viral infection disease is predicted to expand and continue to threaten more lives due to global warming, urbanization, and climate change [2]. Henceforward, tropical infectious diseases should have been an anticipated threat globally [3]. Currently, the available methods used for detecting DENV rely on cell culture [4], PCR [5] and ELISA assays [6]. These conventional diagnosis methods require sophisticated medical facilities as well as trained personnel which are not likely suitable for resource-limited settings [7]. Moreover, DENV is low in particle number during its earlier infection stage, which is a bottleneck for early detection [8,9]. As an alternative, the non-structural protein 1 (NS1) protein of DENV (DENV-NS1) can be used because it holds clinical significance in the early phase [10–12].

Emerging aptamers-based biosensors (aptasensors) have attracted intensive attention in disease diagnostics, environmental monitoring, and surveillance of viral agents [13–15]. Presently, aptamers, a single-stranded oligonucleotide, have been progressively utilized in various fields due to their specific binding with their corresponding target with high affinity. Besides, aptamer possesses several advantages such as ease of chemical functionalization, high stability, and low cost with a little batch-to-batch variation [16]. In terms of simplicity, colorimetric-based aptasensors have been a preferable analytical methods that have been developed using nanozyme [17], localized surface plasmon resonance shift of plasmonic nanomaterial [18], and magnetic nanoparticles [18]. On the contrary, electrochemical-based aptasensor has recently dominated due to its higher signal-transducing properties [19,20]. Unfortunately, the developed methods only provided a single modality assay and may suffer from a lack of signal amplification to establish a highly sensitive detection [21,22].

Several pioneering works utilized liposomal nanoencapsulation to bring multimodal sensing probes into the detection platform, combining optical and electrochemical signal molecules [23,24]. However, the existing nanocarrier has a drawback of its encapsulation uniformity and prolonged protocol due to intermediate steps to activate the sensing probes inside the nanostructure. Conversely, in the previously reported works, utilizing the nanocarrier concept has opened a new approach in developing biosensors to overcome the urgent demand on a wide dynamic range of detection with more complementary information [15,25]. Observing the need for more straightforward detection with higher signal enhancement from the preceding works, a feasible embodiment of intrinsic nanomaterial properties and utilization of nanocarrier are demanded to escalate the performance of the aptasensor.

Gold nanoparticles (AuNPs) have been known to undergo a versatile and easy conjugation of aptamer [26]. Herein, a dual-approach aptasensor was developed to convey a more comprehensive dynamic range of individual detection platforms with a combined feature, highly sensitive detection from an electrochemical signal, and a simple readout from an improved visual change. Coupling of both concepts, nanocarrier and sense-antisense competitive hybridization, the aptasensor was designed and developed to exhibit a competitive colorimetric detection of DENV-NS1 aiming at early-diagnostic, highly sensitive detection of DENV infection. Unlike a conventional single AuNPs-Apt [27], the competitive complementary AuNPs-Apt induced a 3D-nanoassembly structure of AuNPs which demonstrated a higher plasmonic color shift. Different from the general electrochemical aptasensor using an individual conjugated redox probe [28], this finding exploited a nanocarrier-based electrochemical detection by incorporating methylene blue (MB) in the 3D-nanoassembly structure via MB-duplex aptamer interaction. The electrochemical signal from MB proved that it could enhance the detection signal down from picogram to femtogram level. Excitingly, the developed dual-approach aptasensor provided an advanced tool for a sensitive, simple, and label-free DENV-NS1 detection which holds great potential in an early-diagnostic biosensor to target infectious viruses that are very low concentration in the early infection stage.

2. Materials and methods

2.1. Materials, instruments, and preparation of Aptamer conjugated AuNPs (Apt_1-and Apt_2-conjugated AuNPs)

All the above methods are described in detail in **SI-1 Material and Instruments of** the Supplementary data.

2.2. Detection of dengue virus 2 NS1 protein in buffer and spike solution

2.2.1. Colorimetric detection

Dengue virus type 2 NS1 protein (DENV-NS1) was diluted to a series of concentrations. A 50 μL of the DENV-NS1 was mixed into PBS buffer containing $MgCl_2$ (1:1 v/v), and 100 μL of AuNPs-Apt_1 was added into the DENV-NS1 solution. The mixture was incubated for the binding of Apt_1 to the DENV-NS1. The visual color and absorbance were recorded. Next, the mixture was added with 50 μL AuNPs-Apt_2 solution. The mixture was incubated to bind Apt_1 of the AuNPs-Apt_1 and Apt_2 of AuNPs-Apt_2. For the analysis, A_{525} and A_{624} were recorded as the ratio parameter of the detection plot.

2.2.2. Electrochemical detection

The electrochemical detection was conducted on an Apt_2-modified disposable gold electrode (DGE). Apt_2-modified DGE was prepared by incubating 10 μL of 1 μM thiol-functionalized Apt_2. To translate the aptasensor into an electrochemical detection, the AuNPs-Apt complex solution was added with 10 mM methylene blue (MB) solution (1:1 v/v). After incubation, the 15 μL mixture was drop-casted on the Apt_2-modified DGE. Afterward, the solution was discarded, and the DGE was washed several times with PBS buffer containing 1 mM $MgCl_2$. The working solution for the electrochemical detection is PBS buffer with an additional 0.5 M NaCl. The differential pulse voltammetry (DPV) analysis was conducted from − 0.5 V to + 0.2 V at a step potential of 25 mV/s and modulation pulse and time of 50 mV and 50 ms, respectively. The obtained oxidation peak of the DPV was used as the electrochemical signal.

3. Results and discussion

3.1. Mechanism of the 3D-nanoassembled gold nanoparticles aptasensor

The proposed aptasensor was designed based on the aptamer-conjugated AuNPs, forming a competitive binding of AuNPs-Apt_1 to DENV-NS1 and its complementary towards AuNPs-Apt_2. The detection mechanism was designed in two approaches; colorimetric detection and electrochemical detection, as illustrated in Scheme 1. First, AuNPs-Apt_1 were added into the detection sample and bound to the DENV-NS1 via aptamer-DENV-NS1 affinity (**A**). In the presence of DENV-NS1, AuNPs-Apt_1 will bind to the target DENV-NS1, forming AuNPs-Apt_1/DENV-NS1 (**B**). Next, the proposed aptasensor was added the complementary AuNPs-Apt_2 (**C**) to bind to the unbound Apt_1 of AuNPs-Apt_1, forming AuNPs-Apt_1/AuNPs-Apt_2 3D-nanoassembled aggregation (AuNPs-Apt complex) via Apt_1-Apt_2 hybridization (**D**). The induced aggregation

demonstrated the color change depending on the degree of aggregation, which would also be dependent on the DENV-NS1 binding to the Apt_1 on the AuNPs-Apt_1 (AuNPs-Apt complex-based detection).

To utilize the 3D-nanoassembled AuNPs-Apt for electrochemical detection, the methylene blue (MB) was added into the AuNPs-Apt complex **(E)** and bound to the duplex structure of the AuNPs-Apt complex by electrostatical intercalation [29]. Then, on the surface of the DGE, the immobilized Apt_2 aptamer conjugated with the unbound Apt_1 of AuNPs-Apt complex, forming the captured DGE/Apt_2/AuNPs-Apt_1(AuNPs-Apt_2) (DENV-NS1) **(F)**. The MB amount is corresponding to the amount of the hybridized complex of Apt_1 and Apt_2 within the 3D-nanoassembly, inversely proportional to the DENV-NS1 concentration in the sample solution. As the free MB was washed out, the oxidation peak in the DPV analysis indicates the amount of MB carried by the AuNPs-Apt complex only.

3.2. Characterization of the AuNPs-Apt_1, AuNPs-Apt_2, and 3D-nanoassembled AuNPs-Apt complex

Aptamers were conjugated to AuNPs by affinity binding as illustrated in Fig. 1A. AuNPs-Apt_1 was prepared by conjugating biotin-functionalized Apt_1 with streptavidin-functionalized AuNPs and AuNPs-Apt_2 was prepared by indirect method, conjugating via Au-thiol coordination between AuNP with thiolated Apt_2. To confirm the conjugation of the AuNPs-Apt, both functionalized AuNPs were characterized by absorbance, as shown in Fig. 1B. After conjugation with Apt_1 and Apt_2, AuNPs retain their plasmonic properties with peaks at 525 nm with no visible shoulder. In contrast to the single AuNPs-Apt, the mixture demonstrated a change of the absorbance spectra with lower absorbance at 525 nm and immersed the secondary broad peak near 616 nm, indicating the aggregation formation of AuNPs [30]. The image (inset of Fig. 1B) shows that AuNPs-Apt_1 and AuNPs-Apt_2 have red-pinkish color, but the AuNPs-Apt_1/AuNPs-Apt_2 have a blue color, fading in a longer incubation time.

The mixture of AuNPs-Apt_1 and AuNPs-Apt_2 was analyzed under transmission electron microscopy (TEM) to understand the morphology of the aggregation of the AuNP. As shown in Fig. 1C, at first, AuNPs-Apt_1 was visibly well-dispersed with the size of 20 nm. After 5 min, the interaction of AuNPs-Apt_1 and AuNPs-Apt_2 was demonstrated by the initiation of the agglomeration of AuNPs. The aggregation of the AuNPs was evitable in the presence of two AuNPs-Apt. In the conjugation of AuNP-Apt, the size of two AuNPs were different; 20 nm for Apt whereas 5 nm for Apt_2. Due to the difference of AuNPs' sizes, the time course TEM analysis was clearly visible in TEM images (Fig. 1D). In the initial time, single AuNPs-Apt_1 with a size of 20 nm was bound to the individual of AuNPs-Apt_2 with a distinct size of 5 nm. In the longer incubation period, the agglomeration of the combination of 20 nm and 5 nm of AuNPs was clearly visible. Finally, a particular agglomeration degree was observed at a prolonged time where the AuNPs-Apt_1 was shown to be surrounded and bounded by the AuNPs-Apt_2, bridging the AuNPs via aptamer and its anti-sense aptamer [31,32]. It is expected that the AuNPs-Apt_1 and AuNPs-Apt_2 should be capable to bind each other in three-directional formation, resulting the 3D-nano-assemble network of AuNPs.

3.3. The colorimetric detection of DENV-NS1 using the plasmonic shift of AuNPs-Apt_1/AuNPs-Apt_2 aptasensor

The incubation time of AuNPs-Apt_1 were optimized to obtain the highest signal of colorimetric change (Fig. S1). As the incubation time was increased, the binding of AuNPs-Apt_1 was elevated and reached the saturation at 20 min for binding DENV-NS1 (Fig. S1A) and the average of 5 min for the AuNPs-Apt_2 (Fig. S1B). The colorimetric detection of the DENV-NS1 was conducted by a series of concentration of the target analyte. The detection was done starting

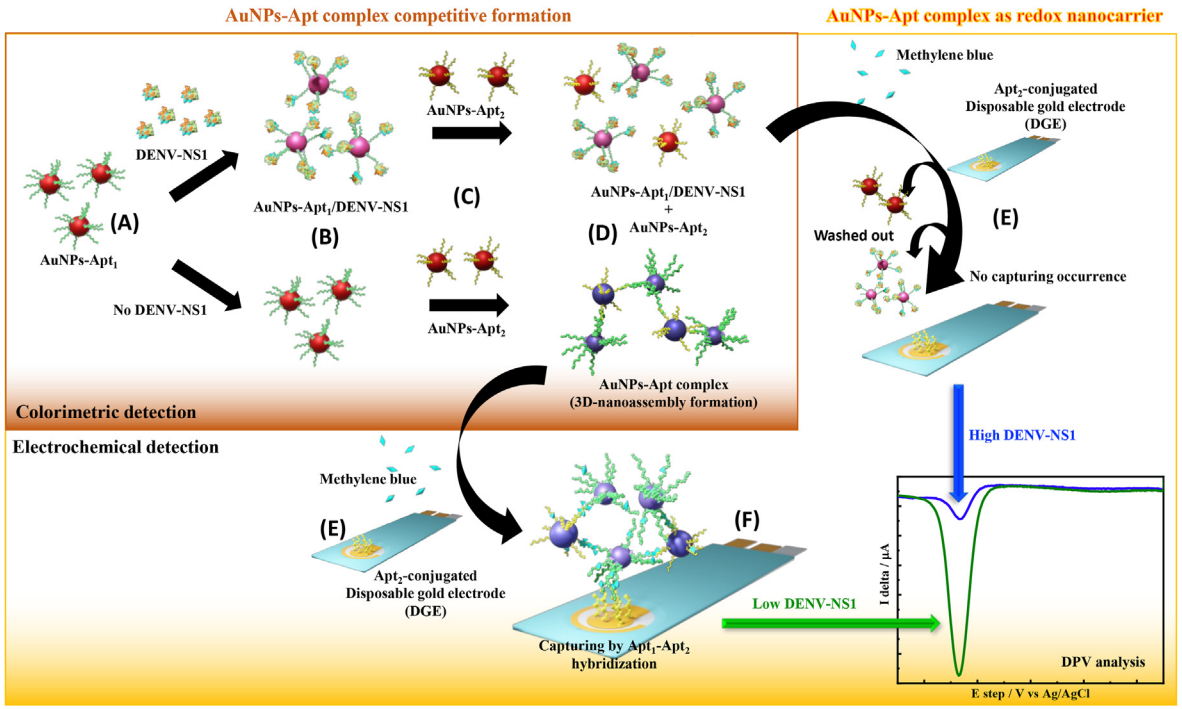

Scheme 1. Proposed 3D-nanoassembled gold nanoparticles-based aptasensor designed for colorimetric detection and electrochemical detection. **(A)** and **(C)** indicate AuNPs-Apt_1 and AuNPs-Apt_2 as the detection probes; **(B)** shows DENV-NS1 binding to AuNPs-Apt_1 and **(D)** shows 3D-nanoassembly of AuNPs; **(E)** indicates electrochemical detection step and **(F)** shows the 3D-nanoassembled AuNPs captured on the Apt_2-modified DGE.

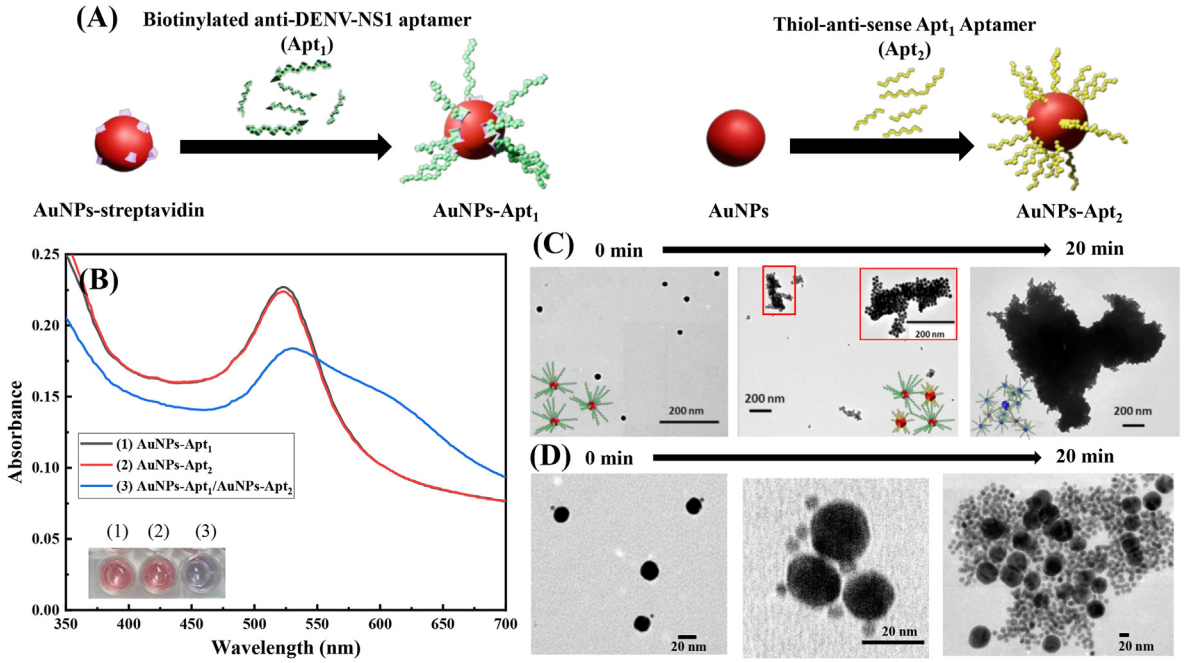

Fig. 1. Characterization of 3D-nanoassembly aggregation of AuNPs-Apt_1 and AuNPs-Apt_2. (**A**) The illustration of the preparation of AuNPs-Apt_1 and AuNPs-Apt_2; (**B**) Absorbance and visual images of the AuNPs-Apt_1 (1), AuNPs-Apt_2 (2) and AuNPs-Apt_1/AuNPs-Apt_2 (3); TEM images of time-dependent nanoassembled formation of (**C**) AuNPs-Apt_1 (20)/AuNPs-Apt_2 (20), and (**D**) AuNPs-Apt_1 (20)/AuNPs-Apt_2 (5). The scale bars of the images are represented on each image.

from the binding step of AuNPs-Apt_1 to DENV-NS1 and continued to binding of AuNPs-Apt_2 to the free Apt_1 on AuNPs-Apt_1. As shown in Fig. 2A, AuNPs-Apt_1 shows a single peak at 525 nm. With the increasing concentration of DENV-NS1, the intensity of the shoulder peak at around 624 nm was also increasing. In addition, the slight shift of the peak maxima was also observed increasing with the DENV-NS1 concentration. Extending from the interaction of AuNPs-Apt_1-DENV-NS1, AuNPs-Apt_2 was introduced to the mixture and intensified the change of the absorbance spectrum. AuNPs-Apt_2 with no DENV-NS1 in the mixture (blank) has elevated shoulder spectra with the lowest absorbance peak at 525 nm (Fig. 2B). These were different in reverse to the AuNPs-Apt_1 after the DENV-NS1 addition. In the addition of AuNPs-Apt_2, the agglomeration of the AuNPs-Apts was promoted since both aptamers would undergo hybridization and lead the 3D-nanoassembly structure of AuNPs [33]. Opposite to the previous trend the interaction of AuNPs-Apt_1 and DENV-NS1, the absorbance showed lower shoulder absorbance with the increasing concentration of DENV-NS1. The absorbance at 525 nm was higher than the control, indicating less aggregation of AuNPs in the system, indicating that the conjugation between AuNPs-Apt_1 and DENV-NS1 was less after-binding to the AuNPs-Apt_2. TEM analysis of the AuNPs-Apt_1/DENV-NS1 and AuNPs-Apt_2 was shown in Fig. S2. Compared to the 3D-nanoassembly formation, the presence of DENV-NS1 prior to the addition of AuNPs-Apt_2 leads to the smaller 3D-nanoassembly formation, preventing to make aggregation of AuNP.

The ratio of A_{525}/A_{624} was plotted from the absorbance spectra as the function of DENV-NS1 concentration. As shown in Fig. 2C, it showed an opposite correlation of the absorbance change of AuNPs-Apt_1 between with the presence of the DENV-NS1, showing positive function, and with the presence of both DENV-NS1 and AuNPs-Apt_2, showing negative function. Based on the absorbance ratio, the direct detection of DENV-NS1 using only AuNPs-Apt_1 showed a detection limit (LOD) of 124.83 pg/mL, based on the 3 times standard deviation and blank signal according to the linearity of the aptasensor [34]. However, the competitive detection by AuNPs-Apt_2 could demonstrate lower LOD, down to 1.28 pg/mL DENV-NS1. Moreover, comparatively to the conventional single aptamer-based aptasensor, AuNPs-Apt complex competitive formation resulted to distinguishable color visual in the presence of the DENV-NS1 by naked eye observation (Fig. 2D). Moreover, after 3.5 weeks of storage, the color change of the AuNPs-Apt_1 did not show any observable change, but AuNPs-Apt_2 did undergo a minor decrease down to a 2.5% change of absorbance (Fig. S3A). The complex AuNPs-Apt was still considerably functional, with detection only down to 6.98% (Fig. S3A). The proposed aptasensor using additional AuNPs-Apt_2 as the anti-sense to promote 3D-nanoassembly of the AuNPs, the advancement strategy showcases an amplified ratiometric for detecting DENV-NS1.

3.4. Electrochemical characterization of 3D-nanoassembled AuNPs-Apt as MB nanocarrier

In search of a more sensitive method, DGE was used as the biosensor platform for easy and straightforward application. First, prior to the detection, the 3D-nanoassembly AuNPs on the DGE was investigated whether it bound to the surface of electrode. The electrochemical impedance spectroscopy (EIS) was conducted to characterize the construction of the 3D-nanoassembled structure on the DGE. DGE showed a typical Nyquist plot of Au-printed electrode (Fig. 3A). After the immobilization of Apt_2 on the DGE (DGE/Apt_2), the impedance of the electrode increased. Next, AuNPs-Apt_1 was captured on the DGE/Apt_2. The layer of AuNPs covers the surface of the DGE and increases its electronic properties, indicated by lower impedance. In contrast, the assembled of AuNPs-Apt_1/AuNPs-Apt_2 complex on the electrode resulted in higher impedance.

The build-up network of the 3D-nanoassembly structure of AuNPs-Apt_1/AuNPs-Apt_2 demonstrated different electronic properties than AuNPs-Apt_1. These indicate that a single layer of AuNPs by AuNPs-Apt_1 had different electronic properties than a 3D-

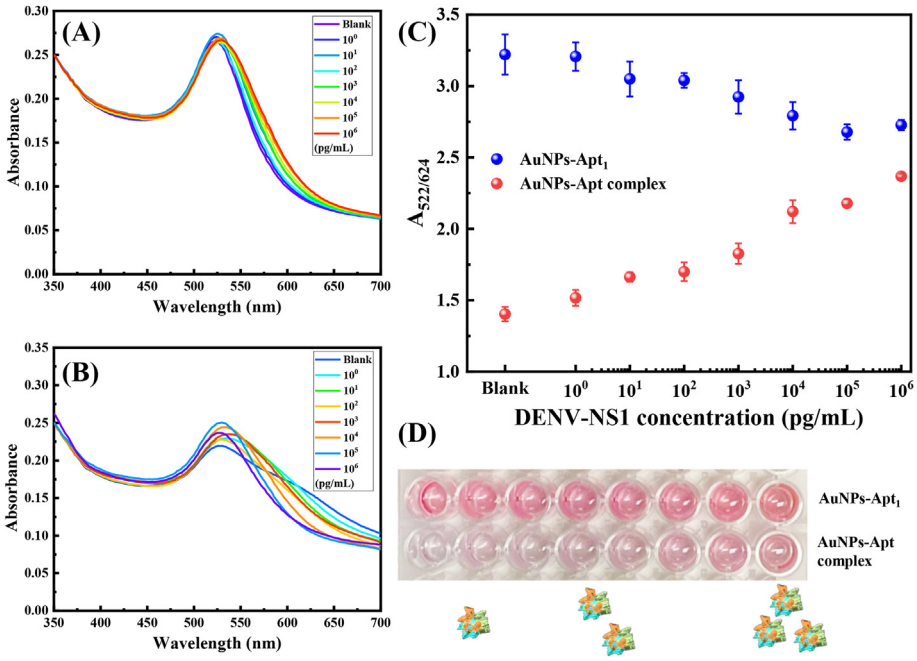

Fig. 2. The colorimetric detection of DENV-NS1 using the proposed aptasensor. The absorbance spectra of the AuNPs-Apt_1 after the addition of DENV-NS1 (**A**) and the addition of DENV-NS1 and AuNPs-Apt_1 (**B**); (**C**) indicates the comparative plot of DENV-NS1 concentration vs. ratiometric of A_{525} and A_{624} (the error bars indicate the standard errors based on three measurements); (**D**) the visual image represents the color change in determining the concentration of DENV-NS1 by the proposed aptasensor. (For interpretation of the references to color in this figure legend, the reader is referred to the Web version of this article.)

nanoassembled structure of AuNPs on the DGE by the aptamer hybridization. In addition, the presence of DENV-NS1 within the 3D-nanoassembled structure had a slightly higher impedance due to the presence of larger biomolecules, such as DENV-NS1.

Further, cyclic voltammetry was applied on the DGE to understand the redox behavior on the surface of the working electrode [35]. As shown in Fig. 3B, an observed peak was in the run with a potential value of around 490 mV which showed a typical reduction-oxidation profile of gold printed electrode [36]. The surface of the DGE was profiled to understand the difference in the presence of AuNPs-Apt_1 and AuNPs-Apt_2. It was observed that DGE/Apt_2/AuNPs-Apt_1 represented the single layer of AuNPs on the DGE has a similar oxidation current like DGE/Apt. However, DGE/Apt_2/AuNPs-Apt_1/AuNPs-Apt_2 resulted the 3D-nanoassembly AuNPs to isolate DGE's surface and unexpectedly lowered the electrons current on the surface of the electrode and reduced the oxidation peak in the cyclic voltammetry profile.

In this mechanism, AuNPs-Apt was acted as nanocarrier for the redox probe, MB in the electrochemical detection. To investigate this, prior to the incubation of AuNPs-Apt_1 and AuNPs-Apt_2 on the DGE/Apt_2, the AuNPs-Apt was incubated in MB solution where the maximum amount of MB can be intercalated inside the aptamer. The loaded amount of the MB was determined from the current value generated in DPV analysis [37] (Fig. 3C). The standard oxidation peak of the MB was founded at −0.28 mV [38]. As Apt_2 was bound to DGE directly, MB molecules chelated and showed higher DPV current than unmodified DGE, increasing from − 3 μA to − 4.5 μA in intensity. This indicates that the Apt_2 was conjugated successfully, and MB was chelated on the capture probe. This is determined here as the noise/background signal in the electrochemical detection. Further, in the presence of captured AuNPs-Apt on the surface of DGE/Apt_2, the DPV analysis indicated a high signal of MB in DGE/Apt_2/AuNPs-Apt_1 and DGE/Apt_2/AuNPs-Apt_1/AuNPs-Apt_2 with the current intensity of − 16 μA and − 27 μA, respectively. Based on the preliminary study from the MB within the AuNPs-Apt, the signal-to-noise ratio was calculated around 3-fold for AuNPs-Apt_1-based nano-assembly and 6-fold for AuNPs-Apt_1/AuNPs-Apt_2-based 3D-nanoassembly structure. These signals were demonstrated to be 2.4% in coefficient of variance on 10 independent DGEs, showing an appropriate signal transducer for the electrochemical aptasensor (Fig. S4). In a control experiment of AuNPs-Apt nanoassembly in absence of MB, it was observed an ignorable hump of oxidation current between potential value of − 250 mV to − 450 mV (Fig. 3D), like the bare DGE's potential value with the current around − 2.5 μA. It is clearly shown that the MB as a redox probe is the only responsible source of current in this electrochemical detection.

3.5. The electrochemical detection of DENV-NS1 using the AuNPs-Apt_1/AuNPs-Apt_2 aptasensor

The electrochemical detection of the DENV-NS1 was carried out after incubating the AuNPs-Apt complex/DENV-NS1 in MB solution. MB's oxidation peak was observed at potential around − 250 mV shown in Fig. 4A. As the concentration of the DENV-NS1 increased, the differential current, known as I delta in DPV analysis (ΔI), increased. Moreover, it was observed the dominant peak from − 250 mV was coupled to peak at potential around −320 mV which represents the MB contribution on DGE. A higher concentration of the DENV-NS1 was resulted to lower the oxidation peak in the DPV, while increasing the I delta value from negative value to less negative value. In absence of target, the conjugated aptamers-AuNPs contain maximum number of MB, resulting strong peak at −250 mV. After gradual increase of DENV-NS1, the peak of MB was decreasing gradually and shifted towards −320 mV, which is the signal of DGE, in presence of MB. In case of high concentration of target DENV-NS1, all apt_1 are completely blocked and there is no space for MB loading on the electrode surface. As a result, the peak intensity in DPV is almost insignificant like the bare electrode without MB. The change of I delta ($\Delta I - \Delta I_{blank}$) at −250 mV was

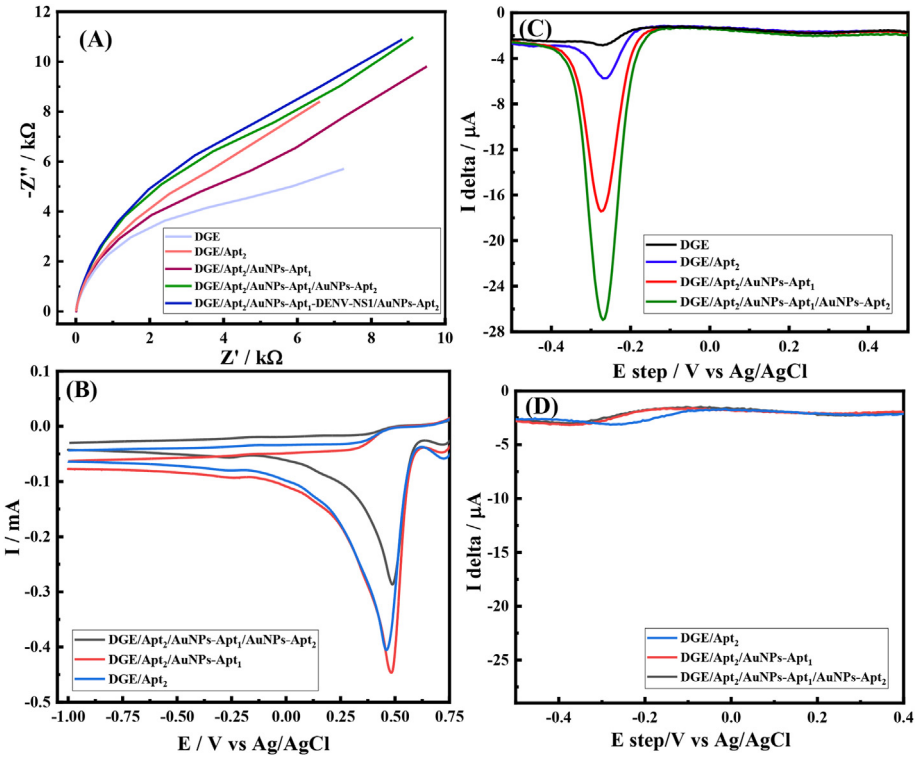

Fig. 3. 3D-nanoassembly AuNPs as the nanocarrier for electrochemical performance on a disposable gold electrode (DGE). (**A**) Electrochemical Impedance Spectroscopy (EIS) and (**B**) Cyclic voltammetry (CV) of the captured AuNPs-Apt_1/AuNPs-Apt_2 on Apt_2-functionalized DGE with scan rate of 75 mV/s; Electrochemical performance of captured 3D-nanoassembly AuNPs-Apt_1/AuNPs-Apt_2 with MB (**C**) and without (**D**). (For interpretation of the references to color in this figure legend, the reader is referred to the Web version of this article.)

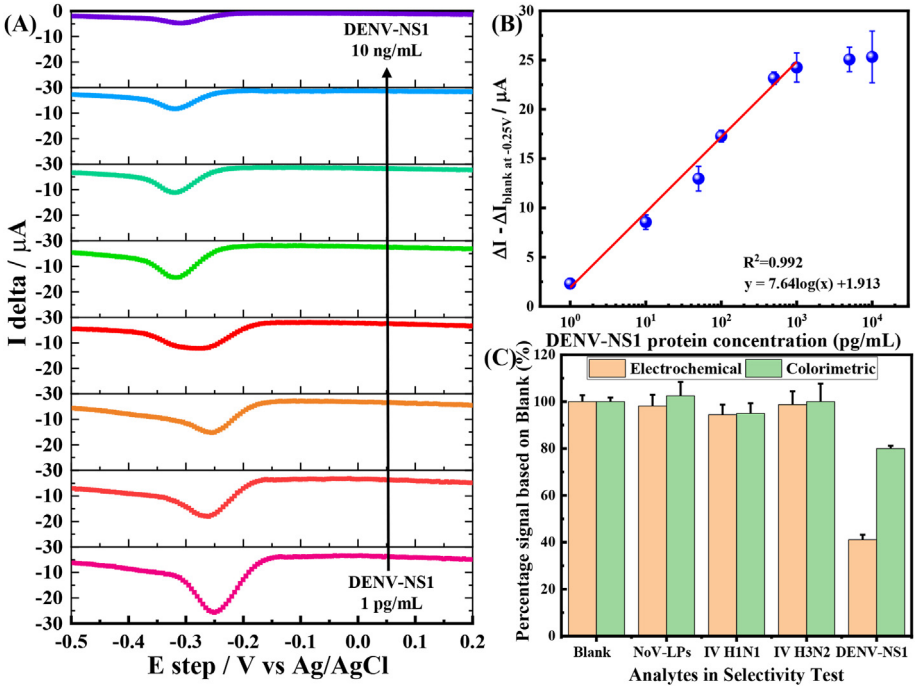

Fig. 4. The electrochemical detection of DENV-NS1 using the proposed aptasensor on Apt_2-immobilized Disposable Gold Electrode (DGE). (**A**) DPV analysis of the aptasensor in response in the DENV-NS1 detection; (**B**) semi-*log* plot of change of differential current (ΔI) vs. concentration of DENV-NS1; (**C**) The selectivity test of proposed aptasensor using colorimetric detection and electrochemical detection. The error bars in **B** and **C** denote the standard errors from three measurements. (For interpretation of the references to color in this figure legend, the reader is referred to the Web version of this article.)

plotted as the function of the concentration of DENV-NS1 (Fig. 4B). The proposed aptasensor demonstrated a linear detection of 1 pg/mL – 1 ng/mL DENV-NS1 with $R^2 = 0.992$. However, over 1 ng/mL DENV-NS1 concentration, it showed to be saturated with a higher cluttering signal observed in a higher-level concentration, where the detection limit was calculated 30 fg/mL, which is 100-times lower than the colorimetric detection. This result emphasizes the advantage of the 3D-nanoassembly structure of AuNPs-Apt as a nanocarrier in the electrochemical detection. A comparative study on previously published works were summarized in Table S1 [39–41], showing that the detection limit of the proposed aptasensor was superior in terms of detection limit and dynamic range.

The selectivity of this dual detection was assayed in 100 pg/mL different non-target analytes, including norovirus-like particles (NoV-LPs), inactivated Influenza virus A/H1N1 and A/H3N2. As shown in Fig. 4C, there is a slight change of signal ranging from 98%–102% based on the blank solution in either of the non-target analytes. However, in the presence of target analytes of 100 pg/mL DENV-NS1, the signal was changed to 80% for colorimetric detection and 40% for electrochemical detection. It showed that even in a picogram concentration of target, electrochemical detection could demonstrate a good specificity towards DENV-NS1. Further, in the spike solution of 2% human serum, the proposed aptasensor could perform well for DENV-NS1 detection with a relative standard deviation (RSD) ranging from 6.1% to 10.2% (Table S2), which was acceptable as the detection variance. However, despite a considerably low RSD value, the developed aptasensor still showed an interfering effect in serum, probably coming from the buffer constituents and the lysate-derived proteins [42]. It was recommendable to minimize the interferences by employing up to 50-fold dilution in the biological complex matrix virus detection as for a pre-treatment and pre-dilution in the practical use.

4. Conclusions

This work reported a dual-detection aptasensor utilizing aptamers-conjugated AuNPs to amplify the signal by 3D-nanoassembled formation. By introducing hybridized duplex aptamer as a bridge of plasmonic aggregation, the 3D-nanoassembled formation intensified the visual color change and provided a nanocarrier function for electrochemical detection. The DENV-NS1 was detected by the disruption of the duplex formation which would prevent the plasmonic color change and redox nanocarrier's moiety of the 3D-nanoassembled AuNPs. It showcased a LOD down to 1.28 pg/mL in colorimetric and 30 fg/mL in electrochemical approaches. Considering the mechanism of the signal amplification, the developed strategy aimed to deliver an elevated concept of the general approach in aptamer-based detection and establishing an early-diagnostic method in low virus concentration or low available biomarker.

CRediT authorship contribution statement

Indra Memdi Khoris: Conceptualization, Methodology, Writing – original draft. **Fahmida Nasrin:** Methodology, Writing – review & editing. **Ankan Dutta Chowdhury:** Data interpretation, Formal analysis, Writing – review & editing. **Enoch Y. Park:** Conceptualization, Writing – review & editing, Supervision.

Declaration of competing interest

The authors declare that they have no known competing financial interests or personal relationships that could have appeared to influence the work reported in this paper.

Acknowledgment

IMK sincerely thank the Japan Society for the Promotion of Science (JSPS) for a research fellowship-DC (20J22358). This work was partially supported by the Fund for the Promotion of Joint International Research, Fostering Joint International Research B (Grant No. 20KK0115) and the Japan Agency for Medical Research and Development (20hm0102080h0001).

Appendix A. Supplementary data

Supplementary data to this article can be found online at https://doi.org/10.1016/j.aca.2022.339817.

References

[1] N. Yanagisawa, K. Wada, J.D. Spengler, R. Sanchez-Pina, Health preparedness plan for dengue detection during the 2020 summer Olympic and Paralympic games in Tokyo, PLoS Neglected Trop. Dis. 12 (2018), e0006755.
[2] F.J. Colón-González, M.O. Sewe, A.M. Tompkins, H. Sjödin, A. Casallas, J. Rocklöv, et al., Projecting the risk of mosquito-borne diseases in a warmer and more populated world: a multi-model, multi-scenario intercomparison modelling study, Lancet Planet. Health 5 (2021) e404–e414.
[3] M.A. Kabir, H. Zilouchian, M.A. Younas, W. Asghar, Dengue detection: advances in diagnostic tools from conventional technology to point of care, Biosensors 11 (2021) 206.
[4] E. Iswardy, T.-C. Tsai, I.-F. Cheng, T.-C. Ho, G.C. Perng, H.-C. Chang, A bead-based immunofluorescence-assay on a microfluidic dielectrophoresis platform for rapid dengue virus detection, Biosens. Bioelectron. 95 (2017) 174–180.
[5] P.R. Abraham, R. Bharathy, P. Kumar, A. Kumar, Dengue NS1 antigen kit shows high sensitivity for detection of recombinant dengue virus-2 NS1 antigen spiked with Aedes aegypti mosquitoes, Sci. Rep. 11 (2021) 23699.
[6] A. Vázquez-Guardado, F. Mehta, B. Jimenez, A. Biswas, K. Ray, A. Baksh, et al., DNA-modified plasmonic sensor for the direct detection of virus biomarkers from the blood, Nano Lett. 21 (2021) 7505–7511.
[7] R. Eivazzadeh-Keihan, P. Pashazadeh-Panahi, T. Mahmoudi, K.K. Chenab, B. Baradaran, M. Hashemzaei, et al., Dengue virus: a review on advances in detection and trends–from conventional methods to novel biosensors, Microchim. Acta 186 (2019) 3249.
[8] S.-C. Lai, Y.-Y. Huang, P.-Y. Shu, S.-F. Chang, P.-S. Hsieh, J.-J. Wey, et al., Development of an enzyme-linked immunosorbent assay for rapid detection of dengue virus (DENV) NS1 and differentiation of DENV serotypes during early infection, J. Clin. Microbiol. 57 (2019), e00221–00219.
[9] O. Parkash, M.A. Abdullah, C.Y. Yean, S.D. Sekaran, R.H. Shueb, Development and evaluation of an electrochemical biosensor for detection of dengue-specific IgM antibody in serum samples, Diagnostics 11 (2021) 33.
[10] A. Dhal, T. Kalyani, S. Ghorai, N.K. Sahu, S.K. Jana, Recent development of electrochemical immunosensor for the diagnosis of dengue virus NSI protein: a review, Sens. Int. (2020) 100030.
[11] D. Wasik, A. Mulchandani, M.V. Yates, Point-of-use nanobiosensor for detection of dengue virus NS1 antigen in adult Aedes aegypti: a potential tool for improved dengue surveillance, Anal. Chem. 90 (2018) 679–684.
[12] P.P.A. Suthanthiraraj, A.K. Sen, Localized surface plasmon resonance (LSPR) biosensor based on thermally annealed silver nanostructures with on-chip blood-plasma separation for the detection of dengue non-structural protein NS1 antigen, Biosens. Bioelectron. 132 (2019) 38–46.
[13] X. Liu, H. Zhang, S. Qin, Q. Wang, X. Yang, K. Wang, Optical fiber amplifier for quantitative and sensitive point-of-care testing of myoglobin and miRNA-141, Biosens. Bioelectron. 129 (2019) 87–92.
[14] Z. Zhang, L. Dong, Q. Zhu, Rational engineering of synergically stabilized aptamer-cDNA duplex probes for strand displacement based electrochemical sensors, Electrochim. Acta 282 (2018) 588–594.
[15] X. Zhang, H. Zhi, M. Zhu, F. Wang, H. Meng, L. Feng, Electrochemical/visual dual-readout aptasensor for Ochratoxin A detection integrated into a miniaturized paper-based analytical device, Biosens. Bioelectron. 180 (2021) 113146.
[16] T.T.-Q. Nguyen, E.R. Kim, M.B. Gu, A new cognate aptamer pair-based sandwich-type electrochemical biosensor for sensitive detection of Staphylococcus aureus, Biosens. Bioelectron. 198 (2022) 113835.
[17] P. Weerathunge, R. Ramanathan, V.A. Torok, K. Hodgson, Y. Xu, R. Goodacre, et al., Ultrasensitive colorimetric detection of murine norovirus using NanoZyme aptasensor, Anal. Chem. 91 (2019) 3270–3276.
[18] L. Xu, R. Chopdat, D. Li, K.T. Al-Jamal, Development of a simple, sensitive and selective colorimetric aptasensor for the detection of cancer-derived exosomes, Biosens. Bioelectron. 169 (2020) 112576.
[19] A. Idili, C. Parolo, R. Alvarez-Diduk, A. Merkoçi, Rapid and efficient detection of the SARS-CoV-2 spike protein using an electrochemical aptamer-based sensor, ACS Sens. 6 (2021) 3093–3101.
[20] S. Sheibani, L. Capua, S. Kamaei, S.S.A. Akbari, J. Zhang, H. Guerin, et al.,

Extended gate field-effect-transistor for sensing cortisol stress hormone, Commun. Mater. 2 (2021) 10.
[21] K. Takemura, A.B. Ganganboina, I.M. Khoris, A.D. Chowdhury, E.Y. Park, Plasmon nanocomposite-enhanced optical and electrochemical signals for sensitive virus detection, ACS Sens. 6 (2021) 2605–2612.
[22] A.B. Ganganboina, A.D. Chowdhury, I.M. Khoris, R.-a. Doong, T.-C. Li, T. Hara, et al., Hollow magnetic-fluorescent nanoparticles for dual-modality virus detection, Biosens. Bioelectron. 170 (2020) 112680.
[23] A.B. Ganganboina, A.D. Chowdhury, I.M. Khoris, F. Nasrin, K. Takemura, T. Hara, et al., Dual modality sensor using liposome-based signal amplification technique for ultrasensitive norovirus detection, Biosens. Bioelectron. 157 (2020) 112169.
[24] F. Nasrin, A.D. Chowdhury, A.B. Ganganboina, O.J. Achadu, F. Hossain, M. Yamazaki, et al., Fluorescent and electrochemical dual-mode detection of Chikungunya virus E1 protein using fluorophore-embedded and redox probe-encapsulated liposomes, Microchim. Acta 187 (2020) 674.
[25] I.M. Khoris, A.B. Ganganboina, E.Y. Park, Self-assembled chromogenic polymeric nanoparticle-laden nanocarrier as a signal carrier for derivative binary responsive virus detection, ACS Appl. Mater. Interfaces 13 (2021) 36868–36879.
[26] R. Gupta, A. Kumar, S. Kumar, A.K. Pinnaka, N.K. Singhal, Naked eye colorimetric detection of Escherichia coli using aptamer conjugated graphene oxide enclosed Gold nanoparticles, Sens. Actuators, B 329 (2021) 129100.
[27] V. Morya, S. Walia, B.B. Mandal, C. Ghoroi, D. Bhatia, Functional DNA based hydrogels: development, properties and biological applications, ACS Biomater. Sci. Eng. 6 (2020) 6021–6035.
[28] C. Wang, Q. Zhao, A reagentless electrochemical sensor for aflatoxin B1 with sensitive signal-on responses using aptamer with methylene blue label at specific internal thymine, Biosens. Bioelectron. 167 (2020) 112478.
[29] E. Farjami, L. Clima, K.V. Gothelf, E.E. Ferapontova, DNA interactions with a methylene blue redox indicator depend on the DNA length and are sequence specific, Analyst 135 (2010) 1443–1448.
[30] A. Baeissa, N. Dave, B.D. Smith, J. Liu, DNA-functionalized monolithic hydrogels and gold nanoparticles for colorimetric DNA detection, ACS Appl. Mater. Interfaces 2 (2010) 3594–3600.
[31] M.Q. He, S. Chen, K. Yao, K. Wang, Y.L. Yu, J.H. Wang, Oriented assembly of gold nanoparticles with freezing-driven surface DNA manipulation and its application in SERS-based MicroRNA assay, Small Methods 3 (2019) 1900017.
[32] M. Luo, M. Xuan, S. Huo, J. Fan, G. Chakraborty, Y. Wang, et al., Four-dimensional deoxyribonucleic acid–gold nanoparticle assemblies, Angew. Chem. Int. Ed. 59 (2020) 17250–17255.
[33] M.-Q. He, S. Chen, K. Yao, J. Meng, K. Wang, Y.-L. Yu, et al., Precisely tuning LSPR property via “peptide-encoded” morphological evolution of gold nanorods for quantitative visualization of enzyme activity, Anal. Chem. 92 (2019) 1395–1401.
[34] I.M. Khoris, A.B. Ganganboina, T. Suzuki, E.Y. Park, Self-assembled chromogen-loaded polymeric cocoon for respiratory virus detection, Nanoscale 13 (2021) 388–396.
[35] A. Dutta Chowdhury, A.B. Ganganboina, F. Nasrin, K. Takemura, R.-a. Doong, D.I.S. Utomo, et al., Femtomolar detection of dengue virus DNA with serotype identification ability, Anal. Chem. 90 (2018) 12464–12474.
[36] V. Rodovalho, G. Araujo, E. Vaz, C. Ueira-Vieira, L. Goulart, J. Madurro, et al., Peptide-based electrochemical biosensor for juvenile idiopathic arthritis detection, Biosens. Bioelectron. 100 (2018) 577–582.
[37] S. Khezrian, A. Salimi, H. Teymourian, R. Hallaj, Label-free electrochemical IgE aptasensor based on covalent attachment of aptamer onto multiwalled carbon nanotubes/ionic liquid/chitosan nanocomposite modified electrode, Biosens. Bioelectron. 43 (2013) 218–225.
[38] S.M. Taghdisi, N.M. Danesh, M.A. Nameghi, M. Ramezani, M. Alibolandi, M. Hassanzadeh-Khayat, et al., A novel electrochemical aptasensor based on nontarget-induced high accumulation of methylene blue on the surface of electrode for sensing of α-synuclein oligomer, Biosens. Bioelectron. 123 (2019) 14–18.
[39] A. Santos, P.R. Bueno, J.J. Davis, A dual marker label free electrochemical assay for Flavivirus dengue diagnosis, Biosens. Bioelectron. 100 (2018) 519–525.
[40] B.B. Junior, M.R. Batistuti, A.S. Pereira, E.M. de Sousa Russo, M. Mulato, Electrochemical aptasensor for NS1 detection: towards a fast dengue biosensor, Talanta 233 (2021) 122527.
[41] M.H. Nawaz, A. Hayat, G. Catanante, U. Latif, J.L. Marty, Development of a portable and disposable NS1 based electrochemical immunosensor for early diagnosis of dengue virus, Anal. Chim. Acta 1026 (2018) 1–7.
[42] J. Tate, G. Ward, Interferences in immunoassay, Clin. Biochem. Rev. 25 (2004) 105.